Solid State Communications 201 (2015) 20–24

Contents lists available at ScienceDirect

Solid State Communications

journal homepage: www.elsevier.com/locate/ssc

Superconducting properties in heavily overdoped $Ba(Fe_{0.86}Co_{0.14})_2As_2$ single crystals

Jeehoon Kim [a,b,*], N. Haberkorn [c], K. Gofryk [d], M.J. Graf [d], F. Ronning [d], A.S. Sefat [e], R. Movshovich [d], L. Civale [d]

[a] CALDES, Institute for Basic Science, Pohang, Republic of Korea
[b] Department of Physics, Pohang University of Science and Technology, Pohang, Republic of Korea
[c] Centro Atómico Bariloche, Bariloche 8400, Argentina
[d] Los Alamos National Laboratory, Los Alamos, NM 87545, USA
[e] Oak Ridge National Laboratory, Oak Ridge, TN 37831, USA

ARTICLE INFO

Article history:
Received 6 August 2014
Accepted 16 September 2014
Available online 5 October 2014

Keywords:
A. Iron arsenide superconductors
B. Upper critical field
C. Magnetic penetration depth
D. Vortex pinning

ABSTRACT

We report the intrinsic superconducting parameters in a heavily overdoped $Ba(Fe_{1-x}Co_x)_2As_2$ ($x=0.14$) single crystal and their influence in the resulting vortex dynamics. We find a bulk superconducting critical temperature of 9.8 K, magnetic penetration depth $\lambda_{ab}(0)=660\pm50$ nm, coherence length $\xi_{ab}(0)=6.4\pm0.2$ nm, and the upper critical field anisotropy $\gamma_{T\to Tc}\approx3.7$. The vortex phase diagram, in comparison with the optimally doped compound, presents a narrow collective creep regime. The intrinsic pinning energy plays an important role in the resulting vortex dynamics as compared with similar pinning landscape and comparable intrinsic thermal fluctuations.

1. Introduction

The discovery of high-temperature superconductivity in the iron–arsenide compounds has motivated discussion of many important physical issues such as the pairing symmetry in the superconducting state, the drastically different magnetic phase diagrams, and the precise nature of the antiferromagnetic spin-density-wave ground state of the parent compound [1]. In addition, iron–arsenide superconductors offer the possibility of improving our knowledge of vortex dynamics for systems showing intermediate properties between low-temperature and high-temperature superconductors. On the other hand, the high critical current density and low anisotropy observed in these systems are promising for technological applications [2,3].

Several theories and models of vortex pinning have been developed for cuprates, where various vortex phase diagrams result from the interplay between vortex fluctuations and different types of pinning centers [4]. Iron based superconductors are characterized by very low pinning energies, and ample range of variations in anisotropy, upper critical fields (H_{c2}), superfluid density [$\rho\sim1/\lambda^2(T)$], and vortex fluctuations (thermal and quantum) [5]. Therefore, its study contributes to a better understanding about vortex matter for both basic and applied research.

Among the iron pnictides superconductors, the family of doped $Ba(Fe_{1-x}Co_x)_2As_2$ (122 family) is one of the most studied compounds due to high quality single crystals available [6,7] The vortex dynamics of this family of pnictides presents elastic to plastic crossover [8,9] deduced from the analysis of J_c as a function of H and T, similar to that found previously in $YBa_2Cu_3O_7$ single crystals [10]. The resulting J_c has been discussed in terms of both typical defects present in as-grown single crystals [11–13] and artificially designed pinning landscapes [14,15]. Beyond the increase of J_c that can be achieved by artificial pinning centers, the comparison between the characteristics of the phase diagram as a function of doping levels are of great importance for understanding the role of intrinsic superconducting parameters on the resulting vortex dynamics [9]. In general, in under and overdoped samples, the superconducting transition width and the superconducting volume are strongly affected by inhomogeneities [16]. In this sense, thermal annealing improves the quality of superconductors, resulting in the enhancement of the superconducting properties [17,18] For example, the heat treatment in $Ba(Fe_{1-x}Co_x)_2As_2$ results in a large suppression of the residual specific heat [17], as well as an increase of the critical temperature T_c.

In this paper we report the influence of intrinsic superconducting properties, such as magnetic penetration depth (λ), upper critical field

* Corresponding author at: CALDES, Institute for Basic Science, Pohang, Republic of Korea and Physics Department, Pohang University of Science, Pohang, Republic of Korea. Tel.: +82 54 279 2077; fax: +82 54 279 9889.
E-mail addresses: jeehoon@postech.ac.kr (J. Kim), haberkornn@yahoo.com.ar (N. Haberkorn), krzysztof.gofryk@inl.gov (K. Gofryk), graf@lanl.gov (M.J. Graf), fronning@lanl.gov (F. Ronning), sefata@ornl.gov (A.S. Sefat), roman@lanl.gov (R. Movshovich), lcivale@lanl.gov (L. Civale).

http://dx.doi.org/10.1016/j.ssc.2014.09.016
0038-1098/

(H_{c2}), and its anisotropy (γ), on the vortex dynamics of annealed $Ba(Fe_{0.86}Co_{0.14})_2As_2$ single crystal. The analysis of the superconducting properties in the extremely overdoped allows a comparison of the resulting vortex dynamics in a material with temperature scales similar to those in conventional superconductors. Other interesting superconducting properties with different vortex features but similar T_c (<10 K) have been previously reported [19,20]. The results here show that γ, λ, and ξ are higher than those in optimally doped single crystals, and the upper critical field anisotropy $\gamma_{T\to T_c}=H_{c2}^{c}/H_{c2}^{ab}\approx 3.7$ is larger than those in lower Co doped single crystals. This material shows a type II superconductivity with $\kappa=\lambda(0)/\xi(0)\approx 103$, and shows intermediate vortex fluctuations between low- and high-temperature superconductors (Ginzburg number, $G_i\approx 4\times 10^{-3}$) [4]. We find that the vortex phase diagram presents similar features to that in the optimal compound, although $J_c(H)$ shows a narrower elastic creep regime [8,9,15]. We attribute this effect to a relatively large coherence length ξ comparable to that found in the optimally doped system above 20 K. Consequently pinning to small crystalline defects is reduced, affecting the vortex creep regimes in the phase diagram.

2. Material and methods

The single crystals were grown by the FeAs/CoAs self-flux method [6]. Details about thermal annealing were discussed in Refs. [17,18]. The λ values were obtained from magnetic force microscopy (MFM) measurements in a home-built low-temperature MFM apparatus [21]. Two Meissner response curves of the $Ba(Fe_{0.86}Co_{0.14})_2As_2$ single crystal and a Nb reference film are directly compared, and hence a direct measurement of the absolute value of $\lambda(T)$ is possible within a single cool-down given the reference value λ^{Nb} of Nb. The $Ba(Fe_{0.86}Co_{0.14})_2As_2$ single crystal and a Nb reference film are loaded simultaneously in a comparative experiment. Details of the experimental technique are described elsewhere [22]. The electrical transport and angular dependence of the critical currents were measured using the Quantum Design (QD) PPMS-9 device equipped with a commercial rotator. A standard four-terminal transport technique was used to measure resistance and I–V curves. The critical current (I_c) was determined using a criterion of 1 μV/cm. In-field I_c measurements were carried out in a maximum Lorentz force configuration ($\mathbf{I}\perp\mathbf{H}$). The magnetization ($\mathbf{M}$) measurements were performed using a QD MPMS-7 setup equipped with a superconducting quantum interference device (SQUID) magnetometer. The critical current densities were estimated by applying the Bean critical-state model to the magnetization data, obtained in hysteresis loops, which is expressed as $J_c=20\Delta M/tw^2(l-(w/3))$, where ΔM is the difference in magnetization between the top and bottom branches of the hysteresis loop, and t (0.1 mm), w (1.5 mm), and l (2 mm) are the thickness, width, and length of the sample ($l>w$), respectively. The flux creep rates, $S=-(d(lnJ_c)/d(lnt))$, were recorded over periods of one hour. The initial time was adjusted considering the best correlation factor in the log-log fitting of the $J_c(t)$ dependence. The initial critical state for each creep measurement was generated by applying a field variation of $H\sim 4H^*$, where H^* is the field for the full-flux penetration [23]. The studied sample presents Meissner response agreement with the geometry.

3. Results and discussion

Fig. 1(a) shows the temperature dependence of the resistance normalized by the value at 300 K. No features of an antiferromagnetic order were observed, which is in agreement with the expectations for overdoped samples [7]. The superconducting transition was determined by considering zero resistance, being 9.8 K (see inset Fig. 1(a)).

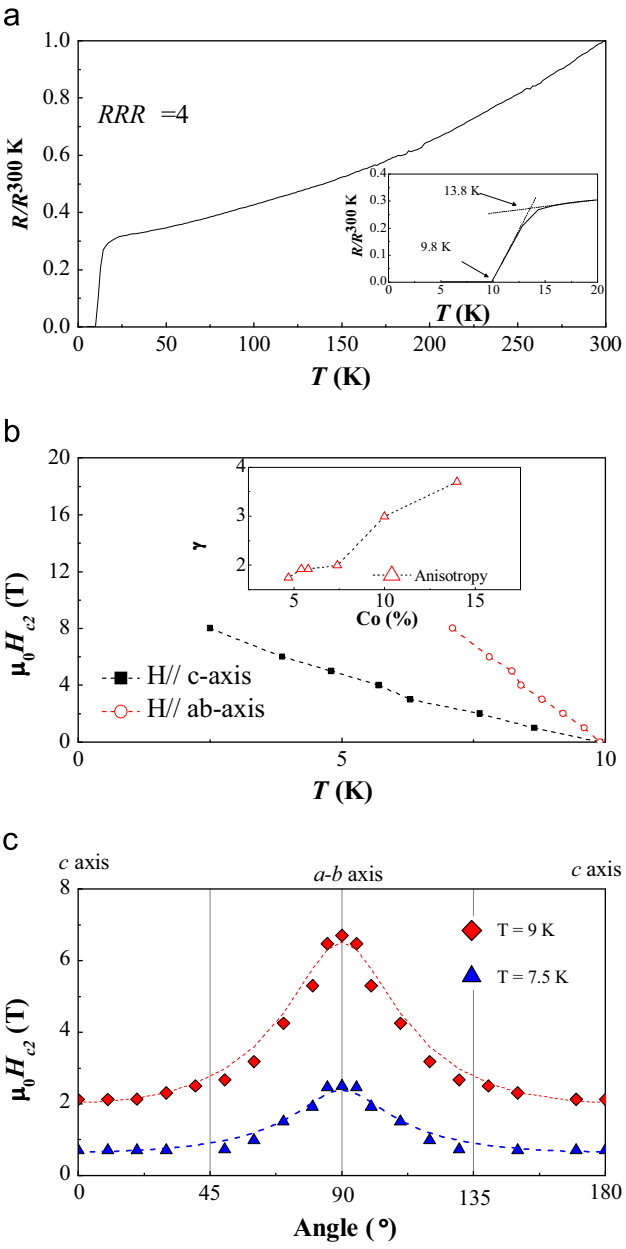

Fig. 1. (a) Temperature dependence of the normalized resistance of an annealed $Ba(Fe_{0.86}Co_{0.14})_2As_2$ single crystal. The inset shows a vicinity of the superconducting transition and the criteria used for the T_c determination. (b) Temperature dependence of the upper critical fields (H_{c2}) in an annealed $Ba(Fe_{0.86}Co_{0.14})_2As_2$ single crystal. Inset shows the Co doping dependence of the anisotropy ($\gamma_{T\to T_c}=H_{c2}^{ab}/H_{c2}^{c}$) taken from Refs. [39,40], and this work. (c) Upper critical field (H_{c2}) versus angle (Θ) at 9 K and 7.5 K. Single-band model [4] calculations with anisotropic scaling are also shown (dashed lines). Same type of fitting at the same T/T_c ratios are obtained by considering H_{irr}.

This value is close to that found by specific heat measurements in a sample of the same batch ($T_c\approx 8$ K indicates that almost $\sim$50% of the volume is superconducting) [17]. The differences on the T_c can be attributed to small differences in chemical composition between samples of the same batch. It is worth to notice that $x=0.14$ is close to the edge of the superconducting dome in the phase diagram, with fast changing T_c, and hence this relatively small chemical gradients lead to large changes of T_c [6,16]. The broadening of the superconducting transition ($\Delta T\approx 4$ K) obtained by electrical transport appears to be an intrinsic characteristic of this compound away from the optimally doped compositions [5]. Thermal fluctuations determine a minimum superconducting transition width, $\Delta T_c\geq G_iT_c$, [4] where G_i

is the Ginzburg number discussed below. For this crystal the result is $\Delta T_c \geq 0.04$ K, thus the much larger $\Delta T_c \sim 4$ K must be due to spatial inhomogeneity. The effect of chemical inhomogeneity is also evident in the $R(T)$ measurements near of the optimally doped composition ($x=0.074$, $\Delta T_c \approx 1$ K) and in overdoped single crystals ($x=0.114$, $\Delta T_c > 2$ K) reported by other authors. Similarly, Harnagea et al. [16] reported a relatively sharp resistive transition for x near optimal doping, but for $x=0.125$ and 0.135 the transition width was ~ 10 K. In our crystal ΔT_c is much smaller even though x is larger, confirming that the annealing tends to reduce the compositional gradients, although some spatial inhomogeneity still remains. It is important to mention that chemical inhomogeneity in iron arsenide materials plays a considerable role in the superconducting transition width and in pinning produced by local reductions in T_c [12]. Fig. 1(b) shows H_{c2} versus T with **H**//c and **H**//ab axis for the studied single crystal. The upper critical fields were determined using the same criteria previously described for T_c (zero resistance). Note that we have not observed an appreciable change in the superconducting transition width with magnetic field, which indicates absence or very narrow vortex liquid phase [4]. To a good approximation in the limit $T \rightarrow T_c$, $H_{c2}(T)$ is linear, with slopes of $-(-(\delta H_{c2}^{ab}/\delta T))|_{T\rightarrow T_c} = 2.8$ T/K and $(-(\delta H_{c2}^{c}/\delta T))|_{T\rightarrow T_c} = 1.15$ T/K. The Werthamer–Helfand–Hohenberg (WHH) expression for a single-band isotropic s-wave superconductor, $H_{c2} \approx -0.69 T_c (\delta H_{c2}/\delta T)|_{T_c}$, by considering the transition width, results in the estimates $H_{c2}^{c} \sim 8\ T$ (in agreement with H_{c2}^{c} at 2.5 K) and $H_{c2}^{ab} \sim 19\ T$, respectively. By using these values, we obtain $\xi_{ab}(0) = 6.4 \pm 0.2$ nm and $\xi_c(0) = 4.0 \pm 0.2$ nm from $H_{c2}^{c} = \Phi_0 / \left[2\pi \xi_{ab}^2(0)\right]$ and $H_{c2}^{ab} = \Phi_0/[2\pi \xi_{ab}(0)\xi_c(0)]$, respectively. However, the $\xi_c(0)$ value estimated by using the WHH expression may be underestimated, since the (Ba,Ca)Fe_2As_2 (122) system presents an unconventional $H_{c2}(T)$ dependence where $\gamma(T)$ is reduced at low temperatures [24,25].

The anisotropy value is $\gamma_{T\rightarrow T_c} = H_{c2}^{c}/H_{c2}^{ab} \approx 3.7$. The inset in Fig. 1(b) displays the Co doping dependence of $\gamma_{T\rightarrow T_c}$, showing an increase in the overdoped region. Since multiband effects could be manifested in the angular dependence of H_{c2} [24], we performed H_{c2} (Θ,T) measurements at 7.5 K and 9 K, as shown in Fig. 1(c). The data may be fit reasonably well by the GL theory of anisotropic 3D superconductors, [4] $H_{c2}(T,\Theta) = H_{c2}(T,\Theta=0)\varepsilon(\Theta)$, where $\varepsilon(\Theta) = [\cos^2\Theta + \gamma^{-2}\sin^2\Theta]^{-1/2}$, and Θ is the angle between the applied magnetic field **H** and the crystallographic c-axis, and by using γ [9 K, $0.91T_c$] ~ 3.7, and γ [7.5 K, $0.76T_c$] ~ 3.3.

The Meissner response measurements were carried out to obtain the magnetic penetration depth λ in $Ba(Fe_{0.86}Co_{0.14})_2As_2$. The magnetic levitation force due to Meissner screening currents is a function of the tip-sample separation z. Data were obtained for both, Nb reference and the $Ba(Fe_{0.86}Co_{0.14})_2As_2$ single crystal [22]. In superconducting single crystals and films whose thickness is larger than λ, the Meissner response force obeys a universal power-law dependence $F(z) \sim (z+\lambda)^{-n}$, where $n=2$ for a magnetic tip in the monopole approximation [26,27]. The frequency shift of the tip resonance is proportional to the gradient of the force, i.e., $\delta f \sim dF(z)/dz$. The λ of Ba$(Fe_{0.86}Co_{0.14})_2As_2$ is obtained by considering the shifting in the Meisner response in comparison with the Nb ($\lambda = 110$ nm): $\lambda^{BFCA}(T) = \lambda^{Nb}(T) + \delta\lambda(T)$, where $\delta\lambda$ is the magnitude of the shift δz [22]. The difference $\delta\lambda$ between Nb and $Ba(Fe_{0.86}Co_{0.14})_2As_2$ is 550 nm at the lowest temperature measured, $T=4$ K, resulting in the approximate zero-temperature value $\lambda^{BFCA}(0\text{ K}) = \lambda^{Nb}(0\text{ K}) + \delta\lambda(0\text{ K}) = 110$ nm + 550 nm = 660 ± 50 nm. Our experimental error is around 10%, resulting from the overlay process of the two Meissner curves of the different λ values: The uncertainty of the λ extrapolation from 4 K to 0 K is as small as a few percent, and thus it is negligible as compared to the main source of the uncertainty of around 10%. The penetration depth (660 nm) has been measured at three locations, separated by 100 μm, resulting in the same values within our experimental uncertainty of 50 nm. Although the large resistive transition width of the system signals the presence of inhomogeneity in the sample, the lack of inhomogeneity in our penetration depth measurement suggests that the length scale of inhomogeneity is far below the size of the scan area (on the order of a micron) which is interrogated (via Meissner force) for determination of the penetration depth. Our MFM result may reflect a "Swiss cheese"-like response of the system to impurities [28], indicating nanoscale inhomogeneity is likely present in the heavily doped $x=0.14$ sample. An alternative possibility could be a granular superconducting behavior, where most of the volume consists of grains with well-developed superconductivity, interconnected by poorly superconducting intra-grain material that acts as "weak links". This behavior tends to occur spontaneously in oxide HTS due to the very small ξ of the order of the lattice parameters. However, this scenario can be ruled out in our case for several reasons. First it is inconsistent with the specific heat data showing a T_c much lower than the onset T_c. Second, the larger ξ in this material precludes the sharp variations in the superconducting properties that occur in granular HTS. Third, in granular materials the inter-grain J_c drops drastically as H increases, that is not the case here as shown below. Thus, the inhomogeneities in this system must be associated with more continuous nanoscale variations in the properties, as expected in the "Swiss cheese" description.

By using $\xi_{ab}(0) = 6.4 \pm 0.2$ nm and $\lambda^{ab}(0) = 660 \pm 50$ nm, we obtain the thermodynamic critical field $H_c(T=0) = \Phi_0/2\sqrt{2}\lambda(0)\xi(0) = 560 \pm 80$ Oe . This value is similar to $H_c \approx 600$ Oe, obtained from the specific heat measurements by integrating the entropy difference between the normal and superconducting states. For this analysis we have used the same approach as described in Ref. [29] for the optimally doped $Ba(Fe_{0.92}Co_{0.08})_2As_2$ [17]. The resulting value for the theoretical critical current density for depairing is $J_0(T=0) = cH_c/3\sqrt{6}\pi\lambda = (3.6 \pm 0.6)$MA cm^{-2}, where c is the speed of the light. This value is approximately 12 times smaller than that for the optimally doped compound [15]. The primary reason for the reduction is the increased λ_{ab}. For comparison, the values of the optimally doped compound are $\lambda_{ab}=260$ nm and $\xi_{ab}=2.6$ nm, respectively [22,25].

The different regimes in the vortex phase diagram of Co-doped $BaFe_2As_2$ single crystals were discussed in Refs. [8] and [9], explaining by the collective pinning theory developed for cuprates [4]. Fig. 2(a) shows the magnetic field dependence of J_c at $T=2$ K, 4.5 K, and 5.5 K, as well as the creep rate, $S = -(d(lnJ_c)/d(lnt))$, at two different temperatures ($T=4.5$ K and 5.5 K). The J_c (H) dependences are characterized by a modulation, resulting from the presence of a mixed pinning landscape, where different type of pining centers are selectively effective in different H ranges, originating from different vortex regimes [15]. Given the geometry of this single crystal ($t=0.1$ mm), we do not observe any clear first regime at low magnetic fields where $J_c(H) \approx$ constant. This regime is typically discussed as the single vortex regime [4], which is strongly affected by self-field effects [30]. In this sample of thickness t, based on $B^*(2\text{ K}) = J_c\, t \approx 500$ Oe and $B^*(4.5\text{ K}) = J_c t \approx 300$ Oe, it is difficult to identify an H range where Te $J_c(H) \approx$ constant. When H is increased, $J_c(H)$ presents a power law dependence, associated with strong pinning centers or large defects [31,32] It should be noted that the pinning associated with these defects depends on the intrinsic superconducting properties (core size and thermal fluctuations). This regime is masked by a third regime, associated with the fishtail or second peak in the magnetization, giving rise to $J_c(H)$ as the sum of two contributions [8,15]. One part is given by large defects or intrinsic pinning (small field) and the other is the fishtail produced by small defects and activated by magnetic fields (large field). The fishtail signature is clear at 2 K, but remains only slightly visible at 4.5 K. The presence of a fishtail has been discussed by several authors, associated with magnetic field induced pinning, where the maximum at the peak is related to a change in the vortex regime [8,10], the so-called elastic to plastic crossover at B^{cr}. From Fig. 2(a) we obtain $J_c(H=0,\ T=2\text{ K}) = 0.05$ MA cm^{-2}, which is $\approx 1.4\%$ of the theoretical depairing current $J_0(T=0\text{ K})$. This small ratio J_c/J_0 is similar to the ratio estimated at 4 K in the optimally doped

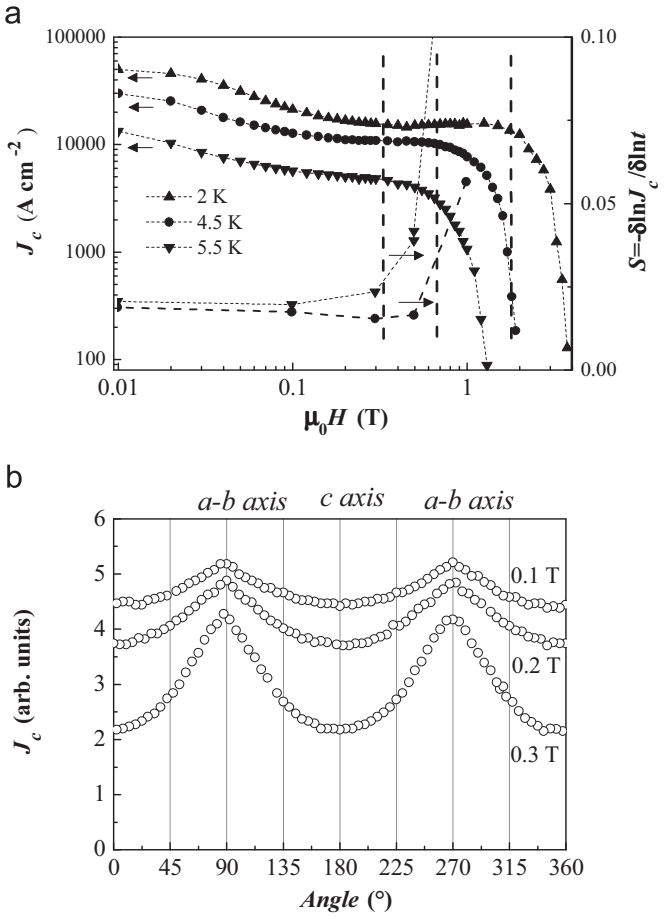

Fig. 2. (a) Magnetic field dependence of J_c and the creep rate $S=-(d(lnJ_c)/d(lnt))$ in the $Ba(Fe_{0.86}Co_{0.14})_2As_2$ single crystal. Vertical dashed lines indicate the fast creep crossover or change in the vortex dynamics regime. (b) Angular dependent critical current density, $J_c(\theta)$ at 9 K and $\mu_0 H=0.1$, 0.2 and 0.3 T in the $Ba(Fe_{0.86}Co_{0.14})_2As_2$ single crystal.

$(Fe_{0.925}Co_{0.075})_2As_2$ single crystals. On the other hand, S values between 0.018 and 0.02 (at 4.5 and 5.5 K and small magnetic fields) can be analyzed by the collective creep theory that considers $S=-(d(lnJ)/d(lnt))=-(T/(U_0+\mu T ln(t/t_0)))$ (here t_0 is a characteristic time, μ the glassy exponent and U_o the barrier height for the flux creep). These S values in these material [9] results from very small U_0 and μ exponents similar to those predicted for cuprates [4].

The presence of a fishtail and the strong suppression of J_c from the ideal value J_0 of the uniform superconductor may be partially understood within the framework of the Swiss cheese model. When Co impurities punch holes into the superconducting order parameter, resembling point-like holes in Swiss cheese, they provide on one side point-like pinning [33,34], but also strongly suppress the local superfluid density due to strong impurity scattering [28,35]. Therefore the similarity between optimally and overdoped samples indicates that large defects, always present in the as-grown samples, produce the same type of pinning at low H. The extension of the collective creep regime, as discussed in Ref. [36], can be associated with the geometry and density of the pinning centers. Thus, we compare the vortex phase diagram between the optimally doped and the under- and overdoped extremes in order to understand the pinning phenomena. Assuming that similar pinning landscapes are obtained in single crystals for the entire doping range, to first approximation, and neglecting thermal fluctuations, the range of the collective pinning regime should be associated with the size of the vortex core and H_c that determine the effectiveness of pinning. In this sense, the features of $J_c(H)$ obtained in the $x=0.14$ sample at low temperatures are similar to those found in optimally doped single crystals ($x=0.075$) above 20 K, which indicates that the pinning by small defects drops when the vortex core size and λ are larger and vortex fluctuation becomes more important [15]. Nakajima et al. [37]. showed that one can improve J_c in Co-doped materials by the introduction of columnar defects (CD). Their results suggest that the crossover temperature from elastic to plastic (fast creep) increases after irradiation, consistent with a non-negligible influence of the ξ-to-defect size ratio and the presence of strong pinning centers, beyond the possible influence of irradiation on the intrinsic superconducting properties [28]. Taking B^{cr}/H_{irr} as a parameter for the comparison, at $0.5T_c$, the near optimally doped sample shows $B^{cr}\approx 0.2H_{irr}$, [9,15] where as in the heavily overdoped sample ($x=0.14$) shows the $B^{cr}\approx 0.06H_{c2}$. We believe that the combined effects of larger ξ and λ values in the overdoped sample significantly suppress the effectiveness of small pinning centers, because of the pinning energy $E_{pin}\sim H_c^2\xi r_d^2$, with r_d the defect size [4]. As a consequence the elastic to plastic crossover is modified. Something similar takes place in the underdoped ($x=0.06$) region [9], where the elastic creep regime is strongly reduced compared to other doping levels with a small ξ [39,40]. In addition, the influence of thermal fluctuations and the $\xi(T)$ dependence on the vortex dynamics are consistent with previously reported data on proton irradiated $Ba(Fe_{0.925}Co_{0.075})_2As_2$ [15]. For $Ba(Fe_{0.86}Co_{0.14})_2As_2$ the strength of the order parameter thermal fluctuations, estimated by the Ginzburg number [4], $G_i=1/2[\gamma T_c/H_c^2(0)\xi^3(0)]^2$ is $G_i\approx 4\times 10^{-3}$, which is of the same order of magnitude with the estimated value for the optimally doped single crystal by using $\gamma_{T\to Tc}$ ($G_i\approx 0.0016$) [15].

In order to analyze the nature of pinning landscape on the plastic regime, we measured the angular dependence of I_c at 9 K and in three different magnetic fields ($\mu_0 H=0.1$, 0.2 and 0.3 T). In this H range, the vortex dynamics is dominated by fast creep rate. Although it is difficult to precisely determine whether the electrical current is homogeneous throughout the sample, these measurements provide information of the pinning center geometry. For example in YBCO films, even in the plastic creep regime, features of correlated pinning, manifested as a peak in J_c when **H**// c-axis, remain at high temperatures. [38] The results presented in Fig. 2(b) indicate the absence of correlated pinning at 9 K, implying that random pinning dominates in the plastic creep regime at high temperatures. In addition, by considering that the pinning at low temperature and below B^{cr} is dominated by large defects, the pinning at 9 K, where ξ_{ab} (9 K) $\approx$ 9 nm, should be dominated by the same type of crystalline defects, suggesting the absence of correlated pinning (such twin boundaries) also at low temperatures.

Fig. 3 shows a simplified H–T vortex phase diagram in the $Ba(Fe_{0.86}Co_{0.14})_2As_2$ single crystal, obtained from magnetization and transport data (no consideration of the pinning potential modulation in the elastic regime). The main characteristic of this phase diagram is its similarity to that describing the vortex dynamics in nearly optimally doped Co-doped $BaFe_2As_2$ [8,9,15]. The phase diagram is characterized by the B_{c2} line and a crossover line (B^{cr}) which separate collective creep (elastic motion) from fast creep (plastic motion). The results presented in this work, in comparison with Refs. [9] and [15], show that the fast creep region is wider than those found in the near optimally doped single crystals. At low H vortices tend to be pinned by the largest defects, e.g., nanoprecipitates, intrinsically appearing in all 122 samples, however, as H increases vortices start to compete and should be pinned collectively by large and small pinning centers together with associated pinning energies. From a geometric point of view alone, one might think that the pinning strength is related to the vortex core to defect size ratio [4]; however the pinning energy of a small point-like defect is controlled by ξ, λ, and r_d, because the

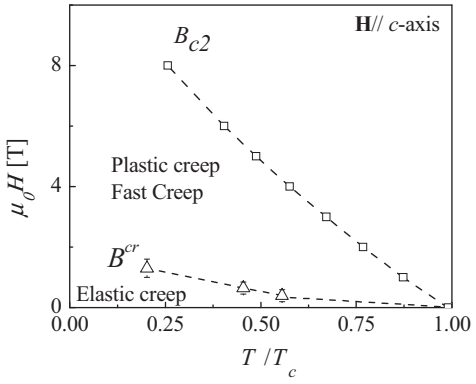

Fig. 3. Normalized temperature dependence of upper critical field (H_{c2}), irreversibility line (H_{irr}) and fast creep crossover (B^{cr}) in the $Ba(Fe_{0.86}Co_{0.14})_2As_2$ single crystal.

pinning energy is given by $E_{pin} \sim H_c^2 \xi r_d^2 \sim r_d^2/\lambda^2 \xi$. In this sense, the pinning by small imperfections should be weaker in under and overdoped samples whose ξ and λ are larger than those in the optimally doped compound [$\xi(0) \approx 2.6$ nm and $\lambda_{ab}(0) \approx 260$ nm].

4. Conclusions

We have measured the absolute value of the zero-temperature magnetic penetration depth $\lambda_{ab}(0)$, upper critical fields $H_{c2}(T)$, and H_{c2} anisotropy γ in the heavily overdoped $Ba(Fe_{1-x}Co_x)_2As_2$ single crystal ($x=0.14$). We found $\lambda_{ab}(0)=660 \pm 50$ nm, $\xi_{ab}(0)=6.4 \pm 0.2$ nm, and $\gamma_{T \to T_c} = 3.7$. No feature of vortex liquid phase has been observed, which is different from the optimally doped compounds with small upper critical field anisotropy. In comparison with the optimally doped compound we have observed that the J_c (H) dependences have similar features with that found above 20 K in the optimally doped compound. This fact can be associated with the larger ξ value which modifies the vortex–defect interaction, and affects the vortex phase diagram by reducing the elastic creep regime at the expense of plastic creep.

Acknowledgments

Research at LANL was supported by the U.S. Department of Energy, Office of and was supported by Institute for Basic Science by Project Code (IBS-R015-D1). N.H. is a member of CONICET (Argentina).

References

[1] J. Paglione, R.L. Greene, Nat. Phys. 6 (2010) 645.
[2] M. Miura, et al., Nat. Commun. 4 (2013) 2499.
[3] K.J. Kihlstrom, et al., Appl. Phys. Lett. 103 (2013) 202601.
[4] G. Blatter, M.V. Feigelman, V.B. Geshkenbein, A.I. Larkin, V.M. Vinokur, Rev. Mod. Phys. 66 (1994) 1125.
[5] T. Tamegai, et al., Rev. Mod. Phys. 25 (2012) 084008.
[6] A.S. Sefat, R.Y. Jin, M.A. McGuire, B.C. Sales, D.J. Singh, D. Mandrus, Phys. Rev. Lett. 101 (2008) 117004.
[7] N. Ni, M.E. Tillman, J.Q. Yan, A. Kracher, S.T. Hannahs, S.L. Bud'ko, P.C. Canfield, Phys. Rev. B 78 (2008) 214515.
[8] R. Prozorov, et al., Phys. Rev. B 78 (2008) 224506.
[9] B. Shen, P. Cheng, Z.S. Wang, L. Fang, C. Ren, L. Shan, H.H. Wen, Phys. Rev. B 81 (2010) 014503.
[10] Y. Abulafia, et al., Phys. Rev. Lett. 77 (1996) 1596.
[11] F. Massee, Y. Huang, R. Huisman, S. de Jong, J.B. Goedkoop, M.S. Golden, Phys. Rev. B 79 (2009) 220517.
[12] S. Demirdis, C.J. van der Beek, Y. Fasano, N.R.C. Bolecek, H. Pastoriza, D. Colson, F. Rullier-Albenque, Phys. Rev. B 84 (2011) 94517.
[13] R. Prozorov, M.A. Tanatar, N. Ni, A. Kreyssig, S. Nandi, S.L. Bud'ko, A.I. Goldman, P.C. Canfield, Phys. Rev. B 80 (2009) 174517.
[14] Y. Nakajima, T. Taen, Y. Tsuchiya, T. Tamegai, H. Kitamura, T. Murakami, Phys. Rev. B 82 (2010) 220504.
[15] N. Haberkorn, et al., Phys. Rev. B 85 (2012) 14522.
[16] L. Harnagea, et al., Phys. Rev. B 83 (2011) 94523.
[17] K. Gofryk, A.B. Vorontsov, I. Vekhter, A.S. Sefat, T. Imai, E.D. Bauer, J.D. Thompson, F. Ronning, Phys. Rev. B 83 (2011) 64513.
[18] K. Gofryk, A.S. Sefat, M.A. McGuire, B.C. Sales, D. Mandrus, T. Imai, J.D. Thompson E.D. Bauer, F. Ronning, J. Phys.: Conf. Ser. 273 (2011) 12094.
[19] Filip Ronning Jeehoon Kim, N. Haberkorn, L. Civale, J.D. Thompson, R. Movshovich, Evgeny Nazaretski, Ni Ni, J.M. Allred, R.J. Cava, Phys. Rev. B 85 (2012) 180504.
[20] T. Klein, H. Grasland, H. Cercellier, P. Toulemonde, C. Marcenat, Phys. Rev. B 89 (2014) 14514.
[21] E. Nazaretski, K.S. Graham, J.D. Thompson, J.A. Wright, D.V. Pelekhov, P.C. Hammel, R. Movshovich, Rev. Sci. Instrum. 80 (2009) 83704.
[22] J. Kim, et al., Supercond. Sci. Technol. 25 (2012) 112001.
[23] Y. Yeshurun, A.P. Malozemoff, A. Shaulov, Rev. Mod. Phys. 68 (1996) 911.
[24] H.Q. Yuan, J. Singleton, F.F. Balakirev, S.A. Baily, G.F. Chen, J.L. Luo, N.L. Wang, Nature 457 (2009) 565.
[25] M. Kano, Y. Kohama, D. Graf, F. Balakirev, A.S. Sefat, M.A. McGuire, B.C. Sales, D. Mandrus, S.W. Tozer, J. Phys. Soc. Jpn. 78 (2009) 84719.
[26] J.H. Xu, J.H. Miller, C.S. Ting, Phys. Rev. B 51 (1995) 424.
[27] M.W. Coffey, Phys. Rev. B 52 (1995) 9851.
[28] J. Kim, N. Haberkorn, M.J. Graf, I. Usov, F. Ronning, L. Civale, E. Nazaretski, G.F. Chen, W. Yu, J.D. Thompson, R. Movshovich, Phys. Rev. B 86 (2012) 144509.
[29] K. Gofryk, A.S. Sefat, E.D. Bauer, M.A. McGuire, B.C. Sales, D. Mandrus J.D. Thompson, F. Ronning, New J. Phys. 12 (2012) 23006.
[30] N. Haberkorn, M. Miura, B. Maiorov, G.F. Chen, W. Yu, L. Civale, Phys. Rev. B 84 (2011) 094522.
[31] C.J. van der Beek, et al., Phys. Rev. B 81 (2010) 174517.
[32] C.J. van der Beek, M. Konczykowski, A. Abal'oshev, I. Abal'osheva, P. Gierlowski S.J. Lewandowski, M.V. Indenbom, S. Barbanera, Phys. Rev. B 66 (2002) 024523.
[33] E.V. Thuneberg, J. Kurkijarvi, D. Rainer, Phys. Rev. Lett. 48 (1982) 1853.
[34] E.V. Thuneberg, J. Kurkijarvi, D. Rainer, Phys. Rev. B 29 (1984) 3913.
[35] T. Das, J.X. Zhu, M.J. Graf, Phys. Rev. B 84 (2011) 134510.
[36] N. Haberkorn, et al., Phys. Rev. B 85 (2012) 174504.
[37] Y. Nakajima, Y. Tsuchiya, T. Taen, T. Tamegai, S. Okayasu, M. Sasase, Phys. Rev. B 80 (2009) 012510.
[38] M. Miura, B. Maiorov, S.A. Baily, N. Haberkorn, J.O. Willis, K. Marken, T. Izumi, Y. Shiohara, L. Civale, Phys. Rev. B 83 (2011) 184519.
[39] K. Vinod, A.T. Satya, S. Sharma, C.S. Sundar, A. Bharathi, Phys. Rev. B 84 (2011) 012502.
[40] NHMFL Annual Report 100, 2011, ⟨http://www.magnet.fsu.edu/mediacenter/publications/reports/2011annualreport/2011-NHMFL-Report100.pdf⟩.